Supporting Information for

Symmetric shear banding and swarming vortices in bacterial superfluids

By Shuo Guo, Devranjan Samanta, Yi Peng, Xinliang Xu, and Xiang Cheng

A. Materials and methods

Bacterial culturing and the construction of the shear cell. We used a fluorescently tagged *Escherichia coli* K-12 strain (BW25113), which carries the PKK_PdnaA-GFP plasmid. The bacteria were cultured overnight (12-13 hours) at 37.0 °C in tryptone broth (TB) culture medium [tryptone 1.2% (w/v), yeast extract 2.4% (w/v), and glycerol 0.4% (v/v)] supplemented with 0.1% (v/v) selective antibiotic (ampicillin 100 mg/L). The saturated culture was diluted 1:100 in TB culture medium and grown at 30.0 °C for 6.5 hours. Cells from 2 ml of culture were harvested by centrifugation at 800*g* for 5 min at room temperature. After discarding the culture medium, 1 ml motility buffer MB+ [0.01M potassium phosphate, 0.067M NaCl, 10^{-4} M EDTA, pH 7.0] containing 0.002% Tween 20 and 0.5% glucose was added to a centrifuge vessel and kept for ~ 1 min. During this time, motile cells moved to the upper layer of the motility medium due to bacterial chemotaxis created by oxygen gradient, whereas immotile cells and bacterial clusters remained at the bottom. The cells in the upper motility buffer were transferred to another centrifuge tube and centrifuged further to high concentrations. To match the density difference between bacteria and the buffer, up to 70% (v/v) Percoll is added into the buffer, which gives us the final *E. coli* suspensions at a concentration of n. The culturing and suspending method allows us to select the most active bacteria with the average velocity at 36 μm/s, crucial for obtaining the swarming phase and the "superfluidic" response of bacterial suspensions.

The activity of *E. coli*—the important factor for sustaining the "superfluidic" phase of bacterial suspensions—decreases with the depletion of oxygen in suspensions. To maintain high bacterial activity at large n, we construct the top plate of the shear cell using a rigid porous membrane of aluminum oxide with pore size 0.02 μm and porosity up to 50% (Anodisc 13, GE Healthcare Life Sciences). The porous membrane allows for the influx of oxygen into the suspensions during experiments, which helps maintain high bacterial activity after a suspension is loaded into the shear cell. The design allows us to study bacterial suspensions at high concentrations above $65n_0$. Nevertheless, the surface of the porous membrane is rough compared with the bottom plate made of microscope coverslips. The difference in the surface properties of the two plates affects bacterial orientations differently and may induce asymmetric shear profiles (see Sec. G below). To eliminate the asymmetric influence of the shear plates on shear profiles, we also construct the top plate using a silicon wafer that is smooth down to nanometer scales. To maintain bacterial activity without O_2, we add an amino acid, L-serine, in bacterial suspensions (1). Via metabolizing L-serine, bacteria exhibit high enough swimming activity for sustaining the state of "superfluids" at intermediate bacterial concentrations between 40 to $65n_0$ (1).

Particle tracking velocimetry (PIV). We used an iterative multigrid approach in our PIV analysis (2). The PIV box size was varied from 24.3 × 24.3 μm^2 down to 6.1 × 6.1 μm^2 in six iterative steps.

www.pnas.org/cgi/doi/10.1073/pnas.1722505115

In most experiments, we directly used fluorescent bacteria as our tracer particles. When bacterial concentrations are low, we also added a small amount of fluorescent polystyrene (PS) spheres as tracers. PIV analysis using bacteria and PS tracers yielded qualitatively similar results. The shear velocities from bacteria are usually slightly smaller than that from PS tracers, indicating relative motions between bacteria and local fluid flows due to active bacterial swimming. The symmetric shear profiles and the measurements on h_s, however, are not affected by the use of different tracer particles.

B. Physical properties of bacterial suspensions

Temporal and spatial variation of bacterial concentrations. We measured the concentration of bacterial suspensions inside suspensions at different heights above the bottom plate. In addition, we also monitored the temporal variation of bacterial concentration over a time interval of 25 min, the maximal time of our experiments. First, we did not observe obvious temporal variation of bacterial concentrations in our samples in the range of bacterial concentrations we studied (Fig. S1A), which excludes strong chemotaxis during our experiments using the porous membrane. Second, the number of bacteria at different heights inside suspensions is approximately uniform with the variation of concentrations across suspensions smaller than 10% (Fig. S1B). We did not observe strong bacterial migration toward the top or bottom walls induced by the applied uniform shear.

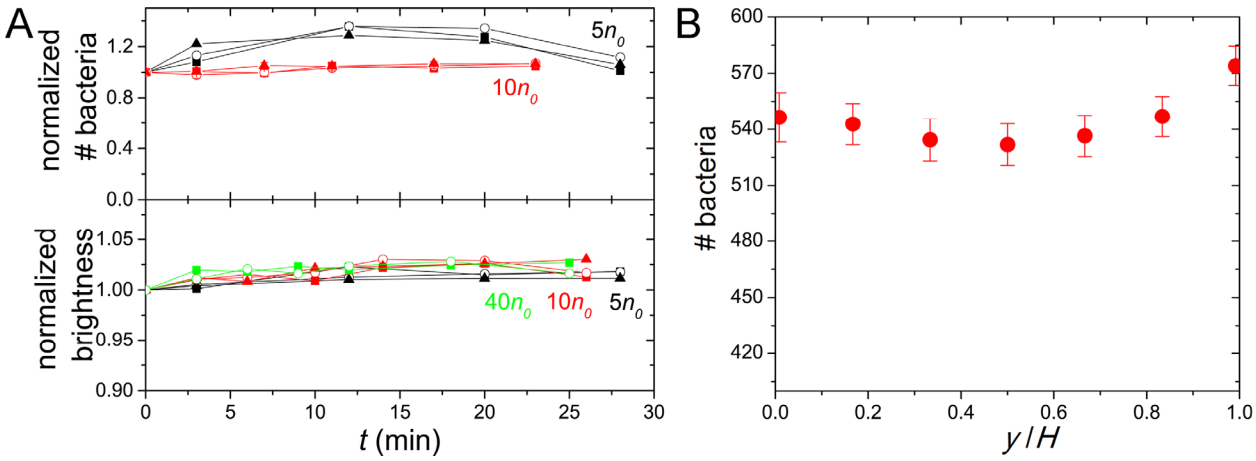

Fig. S1. Bacterial concentration as a function of time at different heights in suspensions. (A) The upper panel shows the number of bacteria through direct counting. The data are normalized by the number of bacteria at t = 0 min. The method can be applied accurately only when bacterial concentrations are low and the contacts and overlaps between bacteria are few. The lower panel shows the light intensity of images, which is proportional to bacterial concentrations. Since bacteria are fluorescently labeled, they show as bright particles in a black background in confocal images (Fig. 1A). The method can be applied to suspensions of higher concentrations. However, it cannot be used to compare different samples or the same sample at different heights due to the lack of proper normalization of light intensity. Bacterial concentrations are indicated with corresponding colors. Solid squares, circles and triangles correspond to y = 10 μm, 30 μm and 50

μm, respectively. Gap thickness H = 60 μm. (B) Number of bacteria at different heights with t < 10 min. $n = 10n_0$ and H = 60 μm.

Density dependence of bacterial swarming. We also measured the enstrophy of bacterial swarming and characterized the size of bacterial swarming vortices at different bacterial concentrations (Fig. S2). The size of swarming vortices is insensitive to the concentration and the swimming speed of bacteria, consistent with previous studies (3, 4), but it depends on the system size as we show in Figs. 6C and D of the main text. In contrast, the enstrophy of bacterial suspension flows depends on the activity of bacterial batches. The results shown in Fig. S2 were obtained from the same bacterial stock. Bacterial activity and therefore the enstrophy of suspensions decreases at very high bacterial concentrations above 140–160n_0 due to the crowding effect, indicating the end of the "superfluidic" behavior at such high bacterial concentrations. In our experiments, we limited the concentration to be below 120n_0.

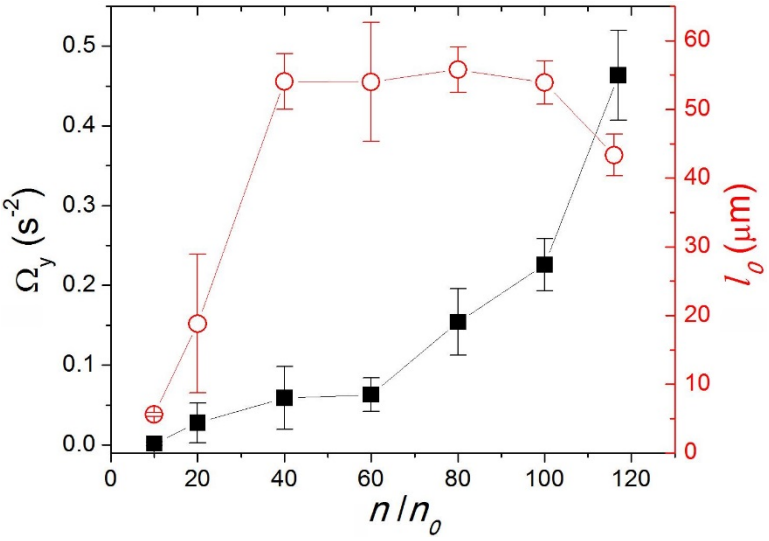

Fig. S2. Enstrophy and size of swarming vortices as a function of bacterial concentrations. The measurements were performed at the center of stationary samples ($y = H/2$) without shear. H = 60 μm. The size of vortices, l, was measured through the spatial velocity–velocity correlation function (Eq. [4] in the main text). Error bars are the standard deviations of three measurements.

Gap size dependence and the nature of 1D confinement. We used two different gap sizes, H = 30 and 60 μm to test the dependence of the shear profiles on the gap thickness. For both gap thicknesses, we observed nonlinear shear profiles. The shear profiles at H = 60 μm have been shown in Fig. 2 of the main text. For H = 30 μm, the shear profiles are less symmetric (Fig. S3). Instead of zero shear gradient near the bottom plate at y = 0, we observe non-zero shear gradients near the bottom plate in some sheared samples. Nevertheless, large shear gradients still concentrate near the center of sheared suspensions. Furthermore, the region of zero shear flow near the top plate is quantitatively similar to the zero flow region at H = 60 μm. Indeed, h_s/H at H = 30 μm follows the same master curve as h_s/H at H = 60 μm (Fig. 3).

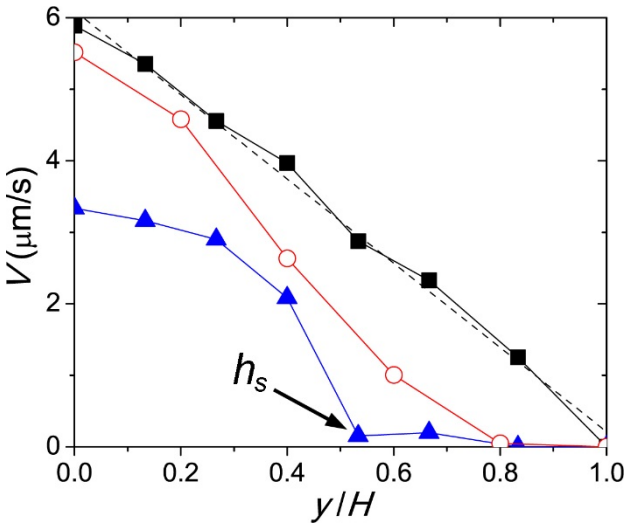

Fig. S3. Shear profiles of bacterial suspensions at H = 30 μm. Bacterial concentration $n = 80n_0$. From top to bottom, the shear rates of the profiles are $\dot{\gamma}_0 = 0.26$, 0.21 and 0.16 s^{-1}, respectively. The dashed line is a linear fit of the shear profile at $\dot{\gamma}_0 = 0.26$ s^{-1}. The stop height, h_s, of the shear profile at $\dot{\gamma}_0 = 0.16$ s^{-1} is indicated.

It is worth of noting that without shear, the mean velocity of our bacterial suspensions is zero. We do not observe the directional flows reported in active fluids under channel (2D) or cavity (3D) confinement (5, 6). The emergence of directional flows breaks the hypothesized ergodicity and satisfies one of the two symmetry-broken nonmonotonic shear profiles shown in Figs. 4B and C. The lack of directional flows in our experiments is due to the nature of the 1D confinement of our experiments. Note that the dimension of our planar Couette cell is ~ 0.1 (y) × 5 (z) × 5 (x) mm^3 along the shear gradient, vorticity and flow directions, respectively. Although bacterial swarming is confined in the shear gradient direction, the active nematic order of active particles is still subject to the instability in the unconfined flow–vorticity plane (7). As a result, bacteria show random swarming in the flow–vorticity plane, eliminating the possibility of directional flows in our system. Our study is more relevant to the rheology of bulk active fluids, where bacterial swarming is isotropic instead of directional (1). The bulk rheology measurements of bacterial superfluids in Ref. (1) used a cylindrical Couette cell with a dimension 0.5 (y) × 8 (z) × 34 (x) mm^3 along the gradient, vorticity and flow directions, respectively. The cell also applies a 1D confinement along the shear gradient direction. Bacterial swarming in the cell should also be random instead of directional.

Thus, the special 1D confinement provided by our shear cell allows us to probe a unique regime of active fluids, where the nonequilibrium "ergodicity" of active fluids manifests as counterintuitive symmetric shear profiles. On the one hand, under the well-explored 2D channel confinement along both the shear gradient and vorticity directions (5, 8), active fluids develop directional flows breaking this ergodic feature. On the other hand, although the unconfined bulk samples are ergodic, they show trivial linear shear profiles as we shall show below in Sec. D, which, therefore, lack a unique experimental signature for detection.

Fitting of shear profiles and measurement of stop height, h_s. We fit our experimental shear profiles piecewise using three linear lines (Fig. S4). The first and the third lines are constant with zero shear rates, whereas the second line has a constant non-zero shear rate. The intersection between the second and the third lines gives the stop height, h_s (Fig. S4C). If shear profiles are linear, we simply fit the profiles with linear lines with $h_s = H$. Fig. S4 show the fitting of the shear profiles shown in Fig. 2 of the main text.

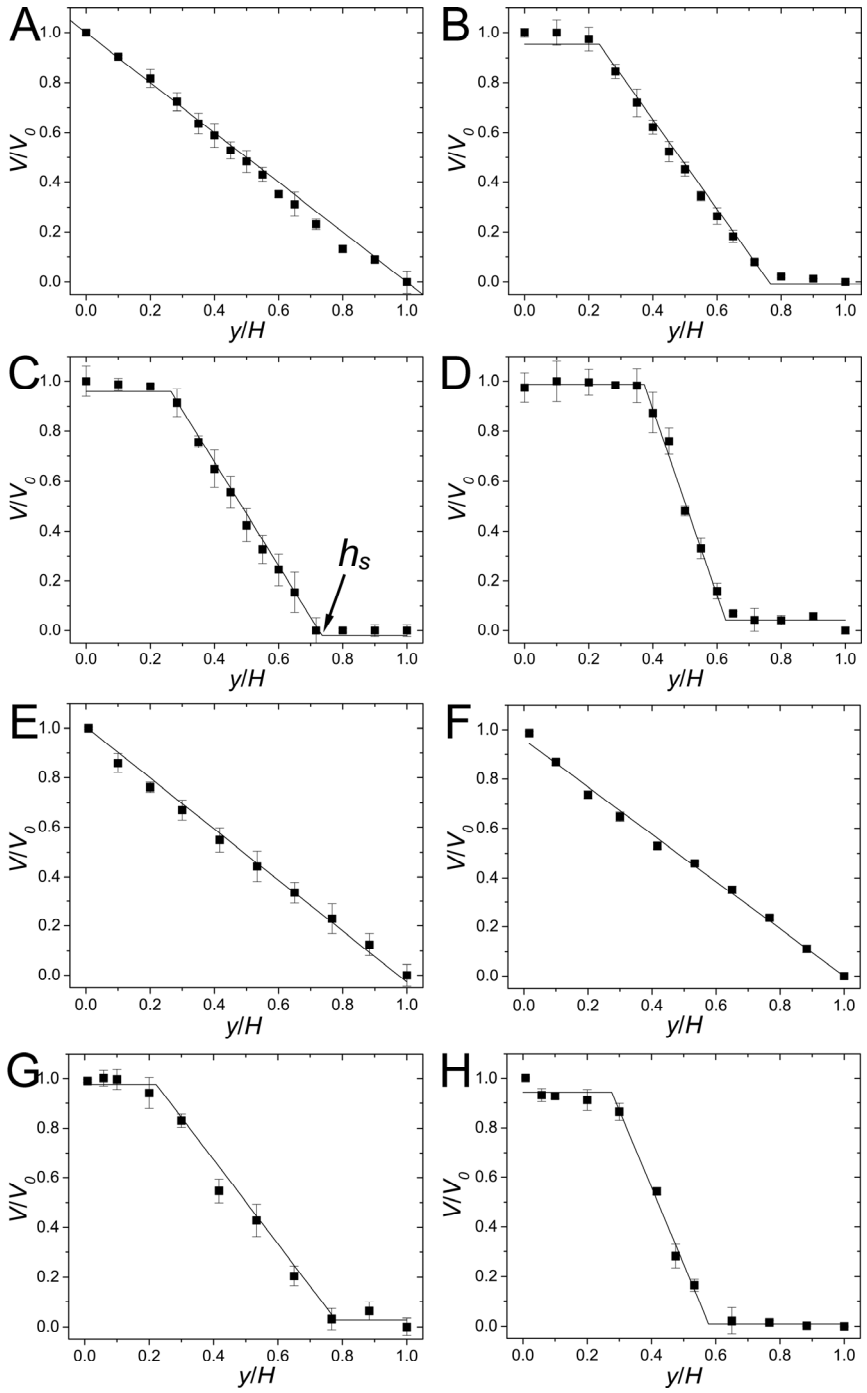

Fig. S4. Fitting of experimental shear profiles with piecewise linear lines. (A)-(D) show shear profiles at a fixed bacterial concentration $n = 50n_0$. (A) $\dot{\gamma}_0 = 0.42$ s^{-1}, (B) $\dot{\gamma}_0 = 0.16$ s^{-1}, (C) $\dot{\gamma}_0 = 0.11$ s^{-1} and (D) $\dot{\gamma}_0 = 0.055$ s^{-1}. (A), (B) and (D) are shown in Fig. 2A of the main text. (E)-(H) show shear profiles at a fixed shear rate $\dot{\gamma}_0 = 0.16$ s^{-1}. (E) $n = 10n_0$, (F) $100n_0$ immobile bacteria, (G) $40n_0$ and (H) $100n_0$. The same data are shown in Fig. 2B of the main text. h_s is defined in (C).

Shear frequency dependence. There are four relevant time scales for bacterial suspensions under oscillatory shear. For bacterial motions, we have (*i*) the tumbling time of individual bacteria and (*ii*) the swarming time of collective bacterial motions. Individual wild-type *E. coli* show a random run-and-tumble motion. The average time interval between two tumbling events is $\tau \sim 1$ s when there is no strong chemotaxis. In contrast, the swarming time arises from the collective motion of many bacteria and is characterized by $1/\sqrt{\Omega_y}$. Our experiments show that the relevant time scale of bacterial motions regulating the sheared dynamics of concentrated bacterial suspensions is $1/\sqrt{\Omega_y}$, instead of τ. For shear flows, we have (*iii*) the time related to shear frequency ($1/f$) and (*iv*) the time related to shear rate ($1/\dot{\gamma}_0 = H/(2\pi Af)$). When combined with the relaxation time of the system, which is given by $1/\sqrt{\Omega_y}$ in the case of concentrated bacterial suspensions, the two different shear time scales give Deborah number (De) and Weissenberg number (Wi) (or equivalently Peclet number if the process is diffusive), respectively. $\mathrm{De} \equiv f/\sqrt{\Omega_y}$ and $\mathrm{Wi} \equiv \dot{\gamma}_0/\sqrt{\Omega_y}$. In our study, we focus on the influence of Wi on the dynamics of bacterial suspensions, which can be changed by either f, A or H independently. We fix the shear frequency $f = 0.1$ Hz. Such a low frequency allows us to approach the quasi-steady shear limit. As a comparison, the swarming time $1/\sqrt{\Omega_y} \sim 1$ s for high concentration bacterial suspensions in the "superfluidic" regime, an order of magnitude smaller than $1/f$. Although at low bacterial concentrations, the swarming time may be comparable or even larger than $1/f$, these suspensions invariantly show trivial linear profiles.

We test the influence of shear frequency on the shear banding structure in the *low*-shear-frequency limit (Fig. S5). The resulting shear profiles are also nonlinear and approximately symmetric. h_s of these profiles quantitatively follows the trend of the master curve obtained at $f = 0.1$ Hz (Fig. 3). To map the entire phase of the dynamics of bacterial suspensions under large amplitude oscillatory shear with De and Wi across a broader range, one needs to construct the so-called Pipkin diagram, which will be the topic of our future research.

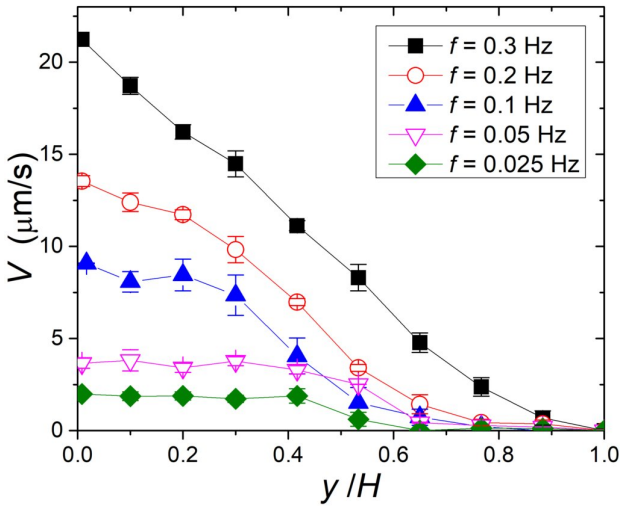

Fig. S5. Shear profiles of bacterial suspensions at different shear frequencies. Bacterial concentration is $n = 80n_0$ and the shear amplitude is $A_0 = 15$ μm.

C. Details on the model of shear banding of active fluids

We calculate the nonmonotonic shear profiles of active suspensions using a simple phenomenological model, where all the quantities in the model (e.g. stresses and bacterial alignment angles) are coarse-grained quantities averaged over local regions that are smaller than the size of swarming vortices but larger than the size of individual bacteria (Fig. S6). In the "superfluidic" phase, we have everywhere in the suspension $\sigma_t = \sigma_s + \sigma_a = 0$, where σ_t is the local total stress, $\sigma_s = \eta\dot{\gamma}_{loc}$ is the local viscous stress with suspension viscosity η and local shear rate $\dot{\gamma}_{loc}$. $\sigma_a = -\zeta Q_{xy}$ is the active stress, where $\zeta > 0$ is a constant indicating the strength of the force dipole bacteria exerted on the suspending fluid and Q_{xy} is the local nematic order parameter of active particles (9). Numerical simulations show that Q_{xy} exhibits a discontinuous jump at $\dot{\gamma}_{loc} = 0$ but is insensitive to $\dot{\gamma}_{loc}$ when $\dot{\gamma}_{loc} > 0$ or $\dot{\gamma}_{loc} < 0$ at low shear rates in the "superfluidic" regime (9). Thus, we approximate Q_{xy} as $Q_{xy} = Q_0\mathrm{sgn}(\dot{\gamma}_{loc})$, where Q_0 is local nematic order measured in stationary suspensions without applied external shear. Since in stationary suspensions, the local shear rate of suspensions is given by the critical shear rate, $\dot{\gamma}^*$ (Fig. 4E) given below, $Q_0 = Q_{xy}(\dot{\gamma}_{loc} = \dot{\gamma}^*)$. A more general consideration of the shear-rate dependent $Q_{xy}(\dot{\gamma}_{loc})$ should not affect the quantitative conclusion of our model (see Sec. F below).

There are two solutions satisfying the zero local stress balance $\sigma_t = \sigma_s + \sigma_a = 0$ with $\dot{\gamma}_{loc} = +\dot{\gamma}^*$ and $-\dot{\gamma}^*$ respectively. Here, $\dot{\gamma}^* \equiv \frac{|\sigma_a|}{\eta} = \frac{\zeta Q_0}{\eta}$ is an intrinsic shear rate of bacterial suspensions. Note that $\dot{\gamma}^*$ is independent of the applied external shear rate, $\dot{\gamma}_0$. Bacterial swarming in stationary samples without shear is completely driven by the active stress. Thus, $|\sigma_a| \approx \eta\omega_y = \eta\sqrt{2\Omega_y}$, which gives $\dot{\gamma}^* = \sqrt{2\Omega_y}$. The argument allows us to bypass the determination of the value of ζ and Q_0 and their dependence on bacterial concentrations and motility. Hence, the instantaneous shear configuration consists of two (or more) shear bands parallel to the confining plates with only two possible shear rates: $+\dot{\gamma}^*$ and $-\dot{\gamma}^*$. If we define w_+ and w_- to be the *normalized* total width of

the bands with the shear rate equal to $+\dot{\gamma}^*$ and $-\dot{\gamma}^*$ respectively, the no-slip boundary conditions at the two confining plates then lead to two simple algebraic relations between w_+ and w_-,

$$w_+ + w_- = 1 \quad \text{[S1a]}$$

$$w_+ - w_- = \eta\,\dot{\gamma}_0/|\sigma_a| = \dot{\gamma}_0/\sqrt{2\Omega_y}. \quad \text{[S1b]}$$

Here, the normalization factor for w_+ and w_- is the gap thickness H. From the above relations, we immediately see that the superfluidic response exists only at small shear rates when $\dot{\gamma}_0/\sqrt{2\Omega_y} \leq 1$, which gives $w_+ = \frac{1}{2}\left(1 + \frac{\dot{\gamma}_0}{\sqrt{2\Omega_y}}\right) \in [0.5, 1]$ and $w_- = \frac{1}{2}\left(1 - \frac{\dot{\gamma}_0}{\sqrt{2\Omega_y}}\right) \in [0, 0.5]$.

Although the values of w_+ and w_- are fixed by Eq. [S1], we have two possible ways to arrange the positions of the two shear bands if we assume there are only two shear bands in the sheared suspensions. In the first configuration, we have the band with the positive shear rate ($+\dot{\gamma}^*$) next to the stationary top plate and leave the band with negative shear rate ($-\dot{\gamma}^*$) next to the moving bottom plate, which leads to the shear profile shown in Fig. 4B. In the second configuration, we have the band with the positive shear rate next to the bottom plate and the band with the negative shear rate next to the top plate, which gives rise to the shear profile shown in Fig. 4C. In both configurations, w_- gives the width of the band with the negative shear rate, i.e., $w_- = w/H$ in the main text. Thus, we reach Eq. [1] of the main text. Note that we have left a constant C on the order of one as a fitting parameter of the model in the main text. Experimentally, we found $C = 1.6 \pm 0.4$.

Since both shear configurations satisfy the stress balance and the no-slip boundary conditions, one cannot select one configuration over the other based on the constraints of the problem alone. Thus, we hypothesize that both shear profiles emerge in sheared suspensions with equal probability. What we measured in experiments *over large spatial areas and long time intervals* should be an average of these two shear profiles. We should emphasize that such an "ensemble" average is different from the coarse-grained average we have performed above to construct the phenomenological hydrodynamic model. A schematic of our modeling procedure may help to illustrate the difference between the two averaging processes (Fig. S6).

How to understand the alternation of two shear configurations and the ergodic assumption physically? First of all, we need to point out that there is a limitation of the 1D continuum model (9). It is known that the nematic order of active pushers is intrinsically unstable. This instability leads to swarming vortices in active pusher suspensions such as bacterial suspensions (7). A constant steady-state shear profile predicted by the 1D continuum model (Fig. 4B and C) with bacteria aligned and moving unidirectionally is inconsistent with this instability. As a side note, under strong channel confinement, the instability can be suppressed, which is the reason why one can observe unidirectional flows of bacterial suspensions in narrow race-track microfluidic channels (5). In this case, the unidirectional steady flow is indeed consistent with the prediction of the 1D model with zero applied shear.

Our experiments, as well as the rheological measurements on bacterial superfluids in the literature (1), do not apply such channel confinement. Thus, bacterial swarming vortices cannot be avoided in these experiments (see e.g. Fig. 1A). Net unidirectional flow does not exist in our experiments.

How to understand the shear banding structure in suspensions, where unidirectional flow is prohibited due to the intrinsic instability of pushers? Is there a way to compromise the bacterial nematic order of the 1D continuum model (9) with the instability theory (7)? We propose here a possible physical interpretation, which naturally leads to the ergodicity of the two shear configurations.

Physically, a single bacterial vortex normal to the flow-vorticity plane extending across the two shear plates (see e.g. vortices shown in Fig. 1A) can be viewed as composed of the two shear configurations predicted by the 1D model (Fig. 4E inset): The half of the vortex moving along the shear direction represents the configuration of Fig. 4B, whereas the other half moving against shear gives the configuration in Fig. 4C. At lengths smaller than the size of a single vortex, the instability is not strong enough to destroy the local bacterial nematic order. Thus, the prediction of the 1D model on shear-banding profiles can be applied.

Since there is no net unidirectional bacterial flows in 3D, the number of bacteria moving against shear has to balance the number of bacteria moving along shear, otherwise bacteria will accumulate at one end of the setup, which we do not observe in our experiments. Thus, to avoid the accumulation of bacteria in any places in the system, on average, the area of regions where bacteria flow against shear has to be the same as the area of regions where bacteria flow along shear. Similarly, the time when bacteria flow against shear needs to be the same as the time when bacteria flow along shear. This argument automatically leads to the ergodic hypothesis. The "ensemble" average of the two shear configurations is therefore achieved experimentally through a spatiotemporal average over multiple swarming vortices. It should be emphasized that swarming vortices are not stationary structures. They constantly change their shapes, which form, move around, disappear and then emerge again in other places. Vortices have a characteristic diameter ~ 60 μm when H = 60 μm (Fig. 1A) and a life time of a few seconds, whereas the spatial and temporal scales of our experiments are much larger at 180 μm and 40 s, respectively.

It is certainly interesting to put the above physical picture into a quantitative theory. Especially, one needs to consider quantitatively how the flows in the voriticity direction modify the shear profile along the shear direction. Such a theoretical development is out of the scope of our current paper.

Lastly, when H is sufficient larger, bacterial suspensions may develop more than two shear bands. In this case, although the total width of all bands with the positive shear rate $\dot{\gamma}^*$ is still w_+ and the total width of all bands with the negative shear rate $-\dot{\gamma}^*$ is still w_-. The detailed configuration of shear profiles and the ensemble average of these shear profiles are more complex. We shall discuss the case of three shear bands as an example in the next section.

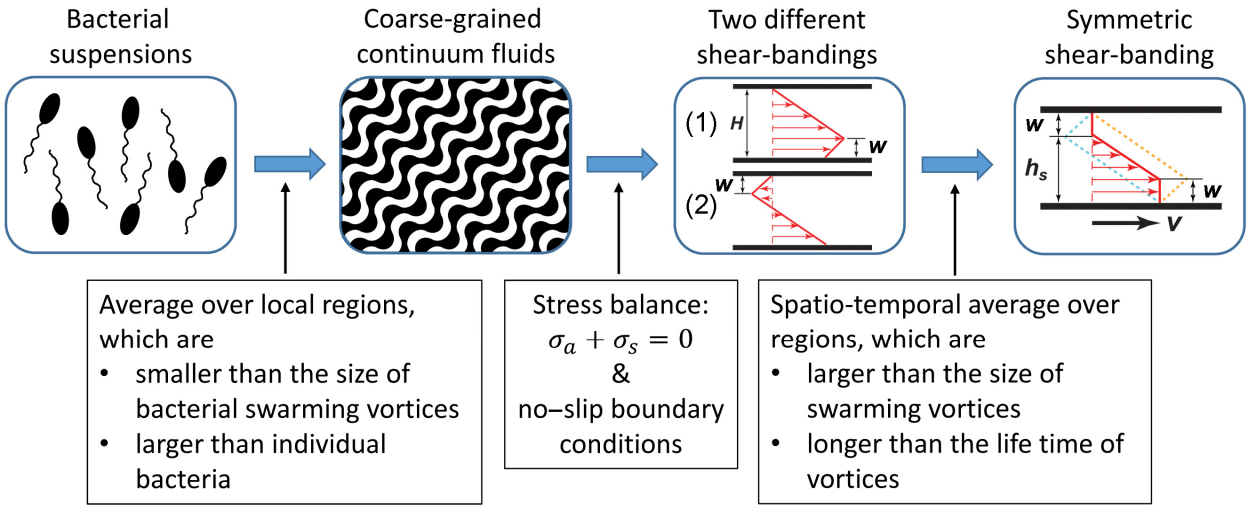

Fig. S6. Schematic showing our model. At short times smaller than the life time of swarming vortices and local regions smaller than the size of swarming vortices but larger than the size of individual bacteria, one should observe one of the two shear-banding structures shown in the third box, i.e., the structures in Figs. 4B and C. At long times and large spatial areas directly accessible in experiments, the average shear profile has the symmetric shear banding structure shown in the last box.

D. Three shear bands

When H is sufficiently large, bacterial suspensions cannot maintain only two shear bands. Multiple shear bands must set in the sheared sample. For all the allowed configurations that have three shear bands, they can be in general sorted into two types, Type A (Fig. S7A) and Type B (Fig. S7B). As we have shown in Sec. C, the total width of all bands with the positive shear rate $\dot{\gamma}^*$ should be w_+ and the total width of all bands with the negative shear rate $-\dot{\gamma}^*$ should be h_-. The value of w_+ and w_- are determined by Eq. [S1]. Thus, the local shear rates for A-type and B-type shear configurations can be parametrized as:

$$\dot{\gamma}_A(y/H, h_1) = \begin{cases} -\dot{\gamma}^*, & 0 < y/H < h_1 \\ \dot{\gamma}^*, & h_1 < y/H < (h_1 + w_+) \\ -\dot{\gamma}^*, & (h_1 + w_+) < y/H < 1 \end{cases} \quad \text{for Type A bands} \qquad [S3a]$$

$$\dot{\gamma}_B(y/H, h_2) = \begin{cases} \dot{\gamma}^*, & 0 < y/H < h_2 \\ -\dot{\gamma}^*, & h_2 < y/H < (h_2 + w_-) \\ \dot{\gamma}^*, & (h_2 + w_-) < y/H < 1 \end{cases} \quad \text{for Type B bands.} \qquad [S3b]$$

Note that $0 < h_1 < w_-$ and $0 < h_2 < w_+$ to satisfy the boundary conditions. Since h_1 and h_2 are continuous variables, there are infinite numbers of allowed configurations.

Under the assumption of ergodicity, we take the ensemble average of the infinite number of shear configurations with equal probability, the shear rate of the averaged shear profile follows

$$\dot{\gamma}_{ave}(y/H) = \int_0^{w_-} \dot{\gamma}_A(y/H, h_1)dh_1 + \int_0^{w_+} \dot{\gamma}_B(y/H, h_2)dh_2, \quad [S4]$$

which leads to $\dot{\gamma}_{ave}(y/H) = \dot{\gamma}_0$, a trivially linear shear profile as we would see in the normal phase. Hence, one will observe the linear profile in a bulk bacterial sample even in the "superfluidic" phase.

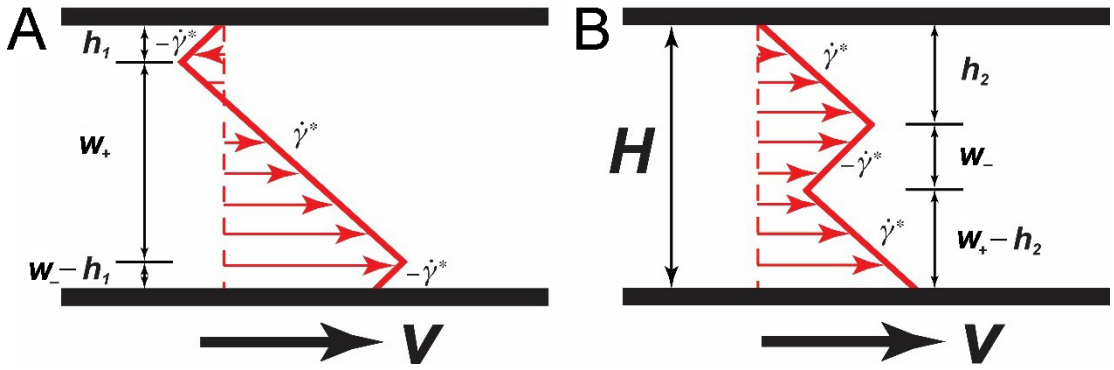

Fig. S7. Shear profiles with three shear bands. (A) Type A shear-banding profile, where the negative shear rates, $-\dot{\gamma}^*$, is next to the moving and stationary plates. (B) Type B shear-banding profile, where the positive shear rate, $\dot{\gamma}^*$, is next to the moving and stationary plates.

Lastly, if the distance between the two plates slightly increases above the strong confinement that allows only two shear bands, it is reasonable to argue that the probability associated with each three-shear-band configuration is quite different from being even. Here, we model the weakly three-shear-band case, where we only allow the configurations with a small third band of a maximal width h_3 near one of the confining plates. The averaged shear profile can then be obtained by changing the integral bounds as

$$\dot{\gamma}_{ave}(y/H) = \frac{1}{4h_3}\left[\int_0^{h_3} \dot{\gamma}_A(y/H, h_1)dh_1 + \int_{w_- - h_3}^{w_-} \dot{\gamma}_A(y/H, h_1)dh_1 + \int_0^{h_3} \dot{\gamma}_B(y/H, h_2)dh_2 + \int_{w_+ - h_3}^{w_+} \dot{\gamma}_B(y/H, h_2)dh_2\right]. \quad [S5]$$

Note that since we assume h_3 is small, it should be smaller than $w_+ \geq 0.5$. Eq. [S5] applies at low shear rates when $h_3 < w_-/2$. For high shear rates when $h_3 > w_-/2$, we need to change h_3 into w_- in the first integral of the equation and modify the normalization factor accordingly. The newly defined average shear profile from Eq. [S5] can be numerically evaluated. Examples are shown in Fig. S8 for $h_3 = 0.1$, corresponding to a third band not to exceed 10% of the total distance between the two plates. These results predict that the existence of h_3 leads to a cross-over between the "superfluidic" and normal phases at small shear rates. Although the calculation predicts the same slope for the linear relation between h_s and $\dot{\gamma}/\sqrt{\Omega_y}$, it is hard to accurately measure h_s at small $\dot{\gamma}/\sqrt{\Omega_y}$ experimentally as the shear profile becomes much smoother at small $\dot{\gamma}/\sqrt{\Omega_y}$ (the black line in Fig. S8).

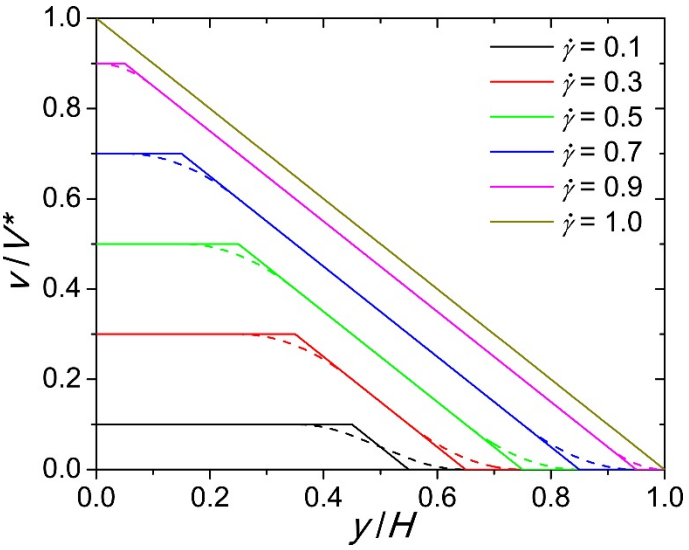

Fig. S8. Average shear profiles with weak three shear bands. Dashed lines are shear profiles with three shear bands. Solid lines are the corresponding shear profiles with two shear bands. The maximal width of the third band is $h_3 = 0.1$. The shear rates are normalized by the characteristic shear rate $\dot{\gamma}^* = \sqrt{2\Omega_y}$. The velocities are normalized by $V^* = \dot{\gamma}^* H$.

E. Fluctuations of local velocities

In the case of two shear bands, the alternation between the two shear configurations shown in Figs. 4B and C leads to the variation of the local suspension velocities at the scale of ~ $l/2$, i.e., the scale of half vortices. l is the size of swarming vortices. Bacteria change the swarming direction by π in each vortex. Conceptually, we can take that a column of a half of the vortex across the bottom and top plates as one of the two shear configurations in Fig. 4. The local velocities measured over a fixed regions of size $l/2$ over a long time should show the fluctuation of the two shear profiles. The fluctuation can be easily estimated by calculating the standard deviation of the two shear configurations around the mean symmetric shear profile. Specifically, assuming the equal probability of the two shear configurations, we have $\langle v_x^2 \rangle = \frac{1}{2} v_{x,l}^2 + \frac{1}{2} v_{x,r}^2$ and $\langle v_x \rangle = \frac{1}{2} v_{x,l} + \frac{1}{2} v_{x,r}$, where $v_{x,r}(y)$ is the suspension velocity at y in the first shear configuration (Fig. 4B) and $v_{x,l}(y)$ is the suspension velocity at y in the second shear configuration (Fig. 4C). The variance of the local velocity at y can then be calculated as $\delta v_x(y) = \sqrt{\langle v_x^2 \rangle - \langle v_x \rangle^2} = \big(v_{x,r}(y) - v_{x,l}(y)\big)/2$, which then yields

$$\delta v_x(y) = \begin{cases} \sqrt{2\Omega_y}\, y & 0 \le y \le w \\ \frac{H}{2}\left(\sqrt{2\Omega_y} - \dot{\gamma}_0\right) & w \le y \le H - w \\ \sqrt{2\Omega_y}(H - y) & H - w \le y \le H \end{cases} \qquad \text{[S6]}$$

in a sheared sample. At the center of the cell $y = H/2$, we have $\delta v_x = \frac{H}{2}\left(\sqrt{2\Omega_y} - \dot{\gamma}_0\right)$, which is Eq. [3] in the main text. Here, we set $C = 1$ in the calculation. The equation shows that the

fluctuation plateaus near the center of the sheared sample and linearly decreases to zero when approaching either the bottom or the top plates. Our measurements of the probability distribution of v_x at y = H/2 quantitatively agree with the above prediction (Fig. 5). Here, we identify $v_{x,l}$ as the left peak of $P(v_x)$ and $v_{x,r}$ as the right peak of $P(v_x)$. The model further predicts that $v_{x,l}$ increases linearly with $\dot{\gamma}_0$ in both the "superfluidic" phase and the normal phase. In comparison, $v_{x,r}$ is constant in the "superfluidic" phase and merges with $v_{x,l}$ in the normal phase. As a result, $\delta v_x(y = H/2)$ decreases linearly with $\dot{\gamma}_0$ in the "superfluidic" phase and reduces to zero in the normal fluid phase. Our experiments quantitatively agree with these predictions (Fig. 5D).

Finally, for stationary samples with $\dot{\gamma}_0 = 0$, Eq. [S6] turns into

$$\delta v_x(y) = \begin{cases} \sqrt{2\Omega_y}y & 0 \le y \le H/2 \\ \sqrt{2\Omega_y}(H-y) & H/2 \le y \le H \end{cases}. \quad [S7]$$

Since $E_{xz} = \delta v_x^2$ when $\dot{\gamma}_0 = 0$, we have

$$E_{xz}(y) = \begin{cases} 2\Omega_y y^2 & 0 \le y \le H/2 \\ 2\Omega_y (H-y)^2 & H/2 \le y \le H \end{cases}, \quad [S8]$$

which predicts a maximum kinetic energy $E_{xz,m} = H^2\Omega_y/2$ at $y = H/2$. $E_{xz,m} \sim H^2$. Our measurements on stationary bacterial suspensions again agree with the prediction (Fig. 6F).

F. Shear-rate dependent active stress. In our simple model, we assume the magnitude of the local nematic ordering of bacteria Q_{xy} and, therefore, the magnitude of active stress are insensitive the magnitude of local shear rates. We demonstrate here that a monotonic decreasing $Q_{xy}(\dot{\gamma})$ shown in (9) does not affect the quantitative prediction of our model. First, as discussed above, the total stress can be written as $\sigma_t = \sigma_s + \sigma_a = \eta\dot{\gamma} - \zeta Q_{xy}(\dot{\gamma})$, where η is the suspension viscosity, $\dot{\gamma}$ is the local shear rate, ζ is a constant indicating the force dipole exerted by active particles and $Q_{xy}(\dot{\gamma})$ is the shear-rate dependent order parameter. Based on $Q_{xy}(\dot{\gamma})$ from (9) (Fig. 1c of the paper), we show schematically the trend of different stress components and the total stress as a function of $\dot{\gamma}$ (Fig. S9).

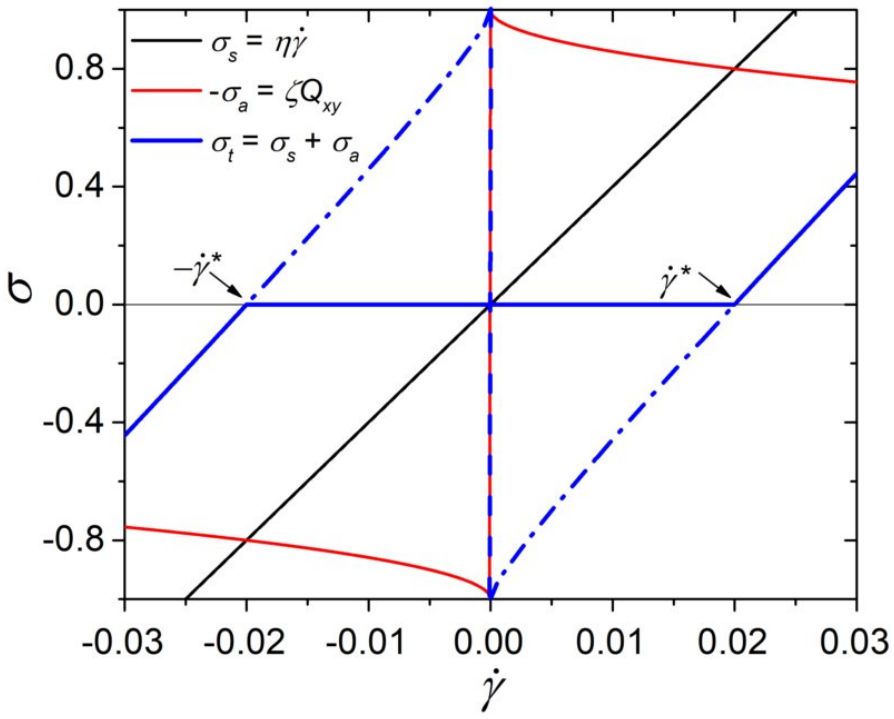

Fig. S9. Stresses of active fluids as a function of local shear rate. The black line shows the viscous stress, $\sigma_s = \eta\dot{\gamma}$. The red line shows the negative of the active stress, $-\sigma_a = \zeta Q_{xy}(\dot{\gamma})$, which is proportional to Q_{xy} shown in Fig. 1c of Ref. (9). The blue line shows the total stress, $\sigma_t = \sigma_s + \sigma_a$. The blue dashed line indicates the unstable regime and the blue dash-dot lines indicate the metastable regime. The critical shear rates, $\dot{\gamma}^*$ and $-\dot{\gamma}^*$, are indicated, where $\sigma_t = \sigma_s + \sigma_a = 0$. Note all the stress components are odd functions of $\dot{\gamma}$.

Since $Q_{xy}(\dot{\gamma})$, and therefore $-\sigma_a$, is a monotonically decreasing function of $\dot{\gamma}$ for $\dot{\gamma} > 0$ (21), the "superfluidic" condition $\sigma_t = \sigma_s + \sigma_a = \eta\dot{\gamma} - \zeta Q_{xy}(\dot{\gamma}) = 0$ has an unique solution at $\dot{\gamma} = \dot{\gamma}^*$ when $\dot{\gamma} > 0$ (Fig. S9), where $\dot{\gamma}^* = \frac{\zeta Q_{xy}(\dot{\gamma}^*)}{\eta} = \frac{|\sigma_a(\dot{\gamma}^*)|}{\eta}$. Since $\sigma_s = \eta\dot{\gamma}$ and $Q_{xy}(\dot{\gamma})$ are both odd functions of $\dot{\gamma}$, there is also a solution at $\dot{\gamma} = -\dot{\gamma}^* < 0$ when $\dot{\gamma} < 0$ (Fig. S9). For $-\dot{\gamma}^* \le \dot{\gamma} \le \dot{\gamma}^*$, an active suspension is "superfluidic" due to the instability induced by the negative slope of $\sigma_t(\dot{\gamma})$ near $\dot{\gamma} = 0$ (9). Note that the blue dashed line with a negative slope is absolute unstable, whereas the blue dash-dot lines are metastable (Fig. S9). The stable total stress at $\sigma_t = 0$ is chosen based on the symmetry of stresses. Such an instability mechanism generally applies for any shear banding fluids (10, 11). In the "superfluidic" phase, a suspension shows a shear-banding flow with two shear bands, which have fixed shear rates, $\dot{\gamma}^*$ and $-\dot{\gamma}^*$, respectively (Fig. 4A). Numerical results of (9) shows $\dot{\gamma}^* = 0.02$ (Fig. 1d of the paper). Similar to our simple model where $|Q_{xy}|$ is a constant, there are two shear-banding configurations that satisfy the no-slip boundary condition at the shear plates with an applied external shear rate $\dot{\gamma}_0$ (Figs. 4B and C). If we still assume the ergodicity of these two shear-banding configurations, we reach,

$$\frac{w}{H} = \frac{1}{2}\left(1 - \frac{\dot{\gamma}_0}{\dot{\gamma}^*}\right) = \frac{1}{2}\left(1 - \frac{\eta\dot{\gamma}_0}{|\sigma_a(\dot{\gamma}^*)|}\right).$$

$|\sigma_a(\dot{\gamma}^*)|$ is exactly what we measure in stationary suspensions. This is because even in stationary samples without applied external shear, the suspensions still develop local shear and the shear-banding structure (Fig. 4E). The local shear is always fixed at the critical shear rate $\dot{\gamma}^*$ or $-\dot{\gamma}^*$, because they are the only solutions of the constitutive equation in the superfluidic phase. Thus, The original relation between the active stress and the enstrophy of stationary samples still applies $|\sigma_a(\dot{\gamma}^*)| = C\eta\sqrt{2\Omega_y}$, where C is a proportional constant serving as a fitting parameter of the model and Ω_y is the enstrophy of stationary suspensions without applied external shear. Hence,

$$\frac{w}{H} = \frac{1}{2}\left(1 - \frac{\dot{\gamma}_0}{\dot{\gamma}^*}\right) = \frac{1}{2}\left(1 - \frac{\eta\dot{\gamma}_0}{|\sigma_a(\dot{\gamma}^*)|}\right) = \frac{1}{2}\left(1 - \frac{\dot{\gamma}_0}{C\sqrt{2\Omega_y}}\right).$$

Finally, the stop height is given by,

$$\frac{h_s}{H} = \frac{1}{2}\left(1 + \frac{\dot{\gamma}_0}{C\sqrt{2\Omega_y}}\right)$$

in the "superfluidic" phase, which is the same as the prediction of our simple model (Eq. (2) of the main text).

In short, the essential component of the hydrodynamic theory is that there are two well-defined symmetric solutions, $\dot{\gamma}^*$ and $-\dot{\gamma}^*$, which give rise to zero total stress. Within $\dot{\gamma}^* \le \dot{\gamma} \le -\dot{\gamma}^*$, any possible variation of active stresses with shear rates, $\sigma_a(\dot{\gamma})$, flattens out due to the mechanical instability induced by the negative slope of $\sigma_t(\dot{\gamma})$ close to $\dot{\gamma} = 0$, a well-known mechanism for the formation of shear-banding flows (10, 11). Such an instability leads to a constant "superfluidic" response with $\sigma_t = 0$, regardless the detailed function form of $\sigma_a(\dot{\gamma})$. Our simple model captures this essential feature and, therefore, can quantitatively predict the behaviors of sheared active fluids.

G. Influence of bacteria-boundary interaction

The presence of solid walls may influence the orientation of bacteria (5) and, therefore, modify the local nematic ordering of bacteria near the walls (12). We generalize our model by considering the influence of the bacteria–boundary interaction below.

When the boundary changes the local nematic ordering of bacteria, the active stress should depend on the height y, which can be written as $\sigma_a = \sigma(y)\mathrm{sgn}(\dot{\gamma}_{loc})$, where the magnitude of the active stress, σ, is now a function of y. $\dot{\gamma}_{loc}$ is the local shear rate. Due to the symmetric boundary condition, σ should be symmetric with respect to the center of the cell, i.e., $\sigma(y) = \sigma(H - y)$, where H is the gap size of the cell. This assumption of the symmetry of $\sigma(y)$ is certainly true for the symmetric smooth shear boundary imposed by the Si wafer where the interactions between bacteria and the top and bottom plates are the same, but is less rigorous when the porous membrane is used as the top plate. The viscous stress is unchanged, $\sigma_s = \eta\dot{\gamma}_{loc}$. The local stress balance in the "superfluidic" phase, $\sigma_a + \sigma_s = 0$, gives two sets of solutions for local shear rates.

$$\dot{\gamma}_1 = \frac{\sigma(y)}{\eta} \quad \text{and} \quad \dot{\gamma}_2 = -\frac{\sigma(y)}{\eta} \qquad \text{[S9]}$$

Since the positive shear rate $\dot{\gamma}_1$ and the negative shear rate $\dot{\gamma}_2$ are both function of y, the shear profiles dictated by Eq. [S9] are no long a combination of linear lines as shown in Figs. 4B and C. Nevertheless, if there are only two shear bands in sheared samples, there are still only two possible shear configurations: Configuration 1 has the positive shear rate $\dot{\gamma}_1$ next to the stationary top wall similar to Fig. 4B, whereas Configuration 2 has $\dot{\gamma}_1$ next to the moving bottom wall similar to Fig. 4C. Since the local shear rate is a smooth function of y, a shear band here is defined as the region where the sign of local shear rate is either positive or negative, instead of a region with a constant shear rate. We shall show next that, to satisfy the no-slip boundary condition, the width of the region with the negative shear rate $\dot{\gamma}_2$, w, is still the same in both shear configurations independent of the function form of $\sigma(y)$.

Since $\dot{\gamma} = dV_x/dy$, for Configuration 1, we have

$$\int_0^{V_0} dV_x = \int_0^{H-w} \dot{\gamma}_1(y)dy + \int_{H-w}^{H} \dot{\gamma}_2(y)dy,$$

where V_0 is the applied shear velocity at the bottom wall. Here, we assign $y = 0$ as the top stationary wall and $y = H$ the bottom moving wall. Thus, we have

$$V_0 = \int_0^{H-w} \frac{\sigma(y)}{\eta} dy - \int_{H-w}^{H} \frac{\sigma(y)}{\eta} dy. \qquad \text{[S10]}$$

If we change the variable to $\tilde{y} = H - y$ and apply $\sigma(y) = \sigma(H - y)$, Eq. [S10] then becomes

$$V_0 = -\int_0^{w} \frac{\sigma(\tilde{y})}{\eta} d\tilde{y} + \int_w^{H} \frac{\sigma(\tilde{y})}{\eta} d\tilde{y}, \qquad \text{[S11]}$$

which can be solved for w if $\sigma(y)$ is given. If $\sigma(y) = |\sigma_a|$ is a constant, we recover Eq. [1] for the simple version of our model without the bacteria–surface interaction in the main text.

Similarly, for Configuration 2, we have

$$V_0 = \int_0^{w} \dot{\gamma}_2(y)dy + \int_w^{H} \dot{\gamma}_1(y)dy = -\int_0^{w} \frac{\sigma(y)}{\eta} dy + \int_w^{H} \frac{\sigma(y)}{\eta} dy,$$

which is the exactly same as Eq. [S11]. Thus, w is the same in Configuration 1 and Configuration 2, independent of the detailed function form of $\sigma(y)$.

Again, assuming the ergodicity of Configuration 1 and 2, we can easily calculate the average velocity of the shear flow. Within $y = [0, w]$, the average velocity is

$$\langle V(y) \rangle = \frac{1}{2}\left[\left(\int_0^{y} \dot{\gamma}_1(y)dy\right) + \left(\int_0^{y} \dot{\gamma}_2(y)dy\right)\right] = 0,$$

which gives a region of zero mean shear velocity near the top stationary wall. The first term in the bracket is the velocity of Configuration 1 at y and the second term is the velocity of Configuration 2 at y. Similarly, within $y = [H - w, H]$, the average velocity is

$$\langle V(y) \rangle = \frac{1}{2}\left[\left(V_0 - \int_y^{H} \dot{\gamma}_2(y)dy\right) + \left(V_0 - \int_y^{H} \dot{\gamma}_1(y)dy\right)\right] = V_0,$$

i.e., a plug flow near the bottom moving wall. Finally, in the region $y = [w, H - w]$,

$$\langle V(y)\rangle = \frac{1}{2}\left[\left(\int_0^y \dot{\gamma}_1(y)dy\right) + \left(\int_0^w \dot{\gamma}_2(y)dy + \int_w^y \dot{\gamma}_1(y)dy\right)\right] = \int_w^y \dot{\gamma}_1(y)dy.$$

The mean shear rate near the center of the shear cell is simply

$$\frac{d\langle V\rangle}{dy} = \dot{\gamma}_1 = \frac{\sigma(y)}{\eta}.$$

Hence, the symmetric shear profile with a stationary region near the top wall and a plug flow near the moving wall, predicted by the simple model, is unchanged when we consider the influence of the bacteria–boundary interaction. Since $\sigma(y)$ is symmetric, it is not surprising that the symmetric feature of the average shear profile preserves.

To quantitatively predict w and therefore the stop height $h_s = H - w$, we need to know the form of $\sigma(y)$, which depends on the detailed interaction between bacteria and solid walls, a topic that is rather complex and still far from well understood (13). Instead of delving into this complicated issue and make extra hypotheses, we argue that the linear relation between h_s and $\dot{\gamma}_0/\sqrt{\Omega_y}$ should be insensitive to $\sigma(y)$ in the "superfluidic" phase. First, it can be easily seen from Eq. [S11] that at the zero shear limit when $V_0 \to 0$, $w \to H/2$ independent of $\sigma(y)$. Second, we can modify Eq. [S11] using the symmetric property of $\sigma(y)$, which gives

$$V_0 = \int_w^{H-w} \frac{\sigma(y)}{\eta} dy. \qquad [S12]$$

Eq. [S12] shows that w only relies on $\sigma(y)$ within the region $[w, H - w]$. Since w approaches $H/2$ in the "superfluidic" phase, this region is very narrow and concentrates near the center of the cell far away from the boundary. It is naturally assumed that the influence of boundary on the nematic ordering of bacteria extends only to a finite length ξ (12), in analogy to the characteristic length in the Frederiks transition of nametic liquid crystals under external magnetic fields (14). Deep in the "superfluidic" phase, $w > \xi$. Thus, in the region $[w, H - w]$, we can assume that $\sigma(y) = \sigma_0$ is a constant. Eq. [S12] then leads to

$$\frac{w}{H} = \frac{1}{2}\left(1 - \frac{\eta V_0}{\sigma_0 H}\right) = \frac{1}{2}\left(1 - \frac{\eta\dot{\gamma}_0}{\sigma_0}\right) = \frac{1}{2}\left(1 - \frac{\dot{\gamma}_0}{C\sqrt{2\Omega_y}}\right), \qquad [S13]$$

where Ω_y is the enstrophy of suspensions in $[w, H - w]$. Eq. [S13] is the same as Eq. [1] obtained from the simple model. Notice that in our experiments, we always measure the enstrophy of bacterial suspensions at the center of the cell $y = H/2$. Ω_y thus obtained reflects the active stress at the center without the influence of the boundary. Near the "superfluidic" transition when w is comparable to ξ, the influence of the boundary cannot be ignored. The linear relation of Eq. [1] cannot quantitatively predict the trend, which may explain the larger scatter of our data near the transition in Fig. 3.

Lastly, considering the influence of the boundary, the variation of velocity fluctuations δv_x should show a nonlinear dependence on y near the boundary, instead of the linear dependence predicted by the simple model in Eq. [S6]. The detailed structure again depends on the function form of $\sigma(y)$. This explains the quantitative deviation of our experimental $E_{xz}(y)$ in Fig. 6E from the theoretical

predictions in Eqs. [S6] and [S8], although qualitatively $E_{xz}(y)$ follows the predictions of the simple model well. Near the center of the cell where the influence of the boundary is weak, the predictions of the simple model on the variation of velocity fluctuations still apply. The linear relation between E_{xz} and Ω_y, between l and H and between E_{xz} and H^2 are all established experimentally at the center of the cell (Figs. 6A, D and F).

References:

1. Lopez HM, Gachelin J, Douarche C, Auradou H, Clement E (2015) Turning Bacteria Suspensions into Superfluids. *Phys. Rev. Lett.* 115:028301.
2. Scarano F, Riethmuller ML (1999) Iterative multigrid approach in PIV image processing with discrete window offset. *Exp. Fluids* 26:513–523.
3. Sokolov A, Aranson IS, Kessler JO, Goldstein RE (2007) Concentration dependence of the collective dynamics of swimming bacteria. *Phys. Rev. Lett.* 98:158102.
4. Sokolov A, Aranson IS (2012) Physical Properties of Collective Motion in Suspensions of Bacteria. *Phys. Rev. Lett.* 109:248109.
5. Wioland H, Lushi E, Goldstein RE (2016) Directed collective motion of bacteria under channel confinement. *New J. Phys.* 18:075002.
6. Wioland H, Woodhouse FG, Dunkel J, Kessler JO, Goldstein RE (2013) Confinement Stabilizes a Bacterial Suspension into a Spiral Vortex. *Phys. Rev. Lett.* 110:268102.
7. Saintillan D, Shelley M (2015) Theory of active suspensions. *Complex fluids in biological systems*, eds. Spagnolie S (Springer-Verlag, New York), pp 319–355.
8. Wu KT, Hishamunda JB, Chen DTN, DeCamp ST, Chang YW, Fernandez-Nieves A, Fraden S, Dogic Z (2017) Transition from turbulent to coherent flows in confined three-dimensional active fluids. *Science* 355:eaal1979.
9. Cates ME, Fielding SM, Marenduzzo D, Orlandini E, Yeomans JM (2008) Shearing active gels close to the isotropic-nematic transition. *Phys. Rev. Lett.* 101:068102.
10. Ovarlez G, Rodts S, Chateau X, Coussot P (2009) Phenomenology and physical origin of shear localization and shear banding in complex fluids. *Rheol. Acta* 48:831–844.
11. Divoux T, Fardin MA, Manneville S, Lerouge S (2016) Shear banding of complex fluids. *Annu. Rev. Fluid Mech.* 48:81–103.
12. Voituriez R, Joanny JF, Prost J (2005) Spontaneous flow transition in active polar gels. *EPL* 70:404–410.
13. Tusona HH, Weibel DB (2013) Bacteria–surface interactions. *Soft Matter* 9:4368-4380.
14. Kleman M, Lavrentovich OD (2003) *Soft Matter Physics: An Introduction* (Springer-Verlag, New York)